Corrosion Product Filled Paste and Corrosion Layer in Reinforced Concrete Beam at Coastal Atmosphere

Xuepeng Lin[1], Jianfeng Dong[1,2,*], Jun Sun[1], Yuxi Zhao[2]

[1]Design and Research Institute Co. Ltd, China Airport Construction Group Corporation, Chengdu, Sichuan, 610200, China
[2]Institute of Structural Engineering, Zhejiang University, Hangzhou, Zhejiang, 310058, China

Abstract. This study investigated the corrosion product filled paste (CP) and corrosion layer (CL) of a beam from a concrete structure at coastal atmospheric environment. The structure was built in 1970s and near the east sea. Part of the beam was cut into several blocks and then polished. The thickness of CP (T_{CP}) and CL (T_{CL}) were observed and measured by scanning electron microscopy. A T_{CP}–T_{CL} model in marine atmosphere is proposed, which provides a mechanistic basis for predicting corrosion evolution and guiding maintenance strategies for aging marine concrete structures. The steel corrosion and values of k_T and T_{CP}^{max}, in the T_{CP}–T_{CL} model of the steel bars, near the windward surface, are larger than those near the leeward surface.

1 Introduction

Corrosion-induced cracking plays a key role in the durability deterioration of reinforced concrete structures [1]. As the steel corrosion develops, the corrosion product produces an expansive pressure on the concrete/steel interface, and result the cracking of concrete cover [2]. Once cracking, aggressive agents can ingress into the concrete from the cracks and accelerate the steel corrosion, which will result in durability deterioration, and structure failure at last[2].

The steel corrosion product was divided into two parts in previous studies: corrosion-product-filled paste (CP) and corrosion layer (CL) [3-5]. CP is an area that the corrosion products penetrated into the near concrete and doesn't produce expansion pressure. CL is the corrosion products accumulated at the steel–concrete interface and produces expansion pressure on the surrounding concrete.

Previous studies by the authors [5] observed the steel/concrete interface by SEM. The specimens were accelerated corroded in the NaCl solution by wet and dry cycles or by electricity. Both results (specimens corroded by wet and dry cycles and by electricity) show that the thickness of CP (T_{CP}) increases with the thickness of CL (T_{CL}) at the beginning, and then T_{CP} no longer increase as the increasing of T_{CL}. The model was proposed as shown in Fig. 1.

In recent years, X-ray computed tomography is widely applied to study the steel corrosion behavior in concrete. Wang [6] use X-ray computed tomography to scan the magnesium oxychloride cement concrete, and use scanning electron microscope (SEM) study the interface transition zone. They found CP is needle-shaped, which causes the formation of a weak surface in the interfacial transitional zones so that corrosion-induced cracks usually develop along those zones.

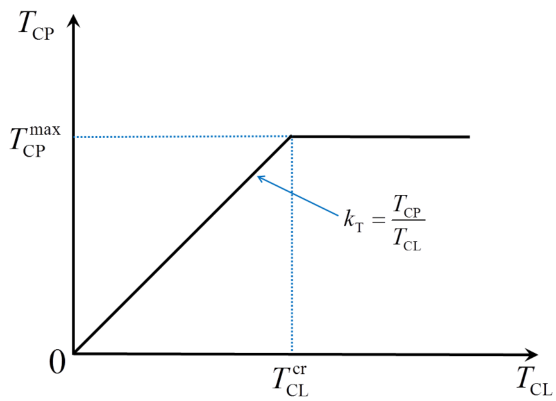

Fig. 1. T_{CP}–T_{CL} model in reference [5]

Robuschi [7] and Tian [8] develop the post-process following XCT scanning to quantifying steel corrosion. Based on the image thresholding method, the picture of steel/concrete interface can be divided into different phases automatically[3]. Wang [9] proposed a novel method for quantifying the filling proportion of corrosion products β_F at the macro- and meso-scales using X-ray computed tomography and image segmentation algorithms. They found that there is a positive correlation between β_F and corrosion propagation, moisture content in the environment, and β_F was negatively associated with concrete cover thickness.

However, the specimens tested in order to investigate the T_{CP}–T_{CL} model are very limited. Previous studies[5] corroded the specimens by electricity or dry/wet cycle and unload. Few study was carried out on actual structures under natural environment under loading.

*djf_1991@126.com

Obviously, loads could influence the steel corrosion produce and even the surrounding concrete[10].

Therefore, the thickness of CP and CL at the steel/concrete interface of a beam serviced in a structure under coastal atmospheric environment was studied. The T_{CP} and T_{CL} were detected and analyzed. The T_{CP}–T_{CL} model is proposed. This study provides a mechanistic basis for predicting corrosion evolution and guiding maintenance strategies for aging marine concrete structures.

2 Experimental Program

2.1 The Concrete Beam

The beam used in the study was from a structure built in 1970s exposed to coastal atmospheric environment. The relationship between the beam and the environment was shown in Fig.2. The length of beam was about 3 meters, and only about 1400 mm was used in the study because the other parts was damaged severely. The beam was removed from the structure in 2015, and then it was stored in the lab.

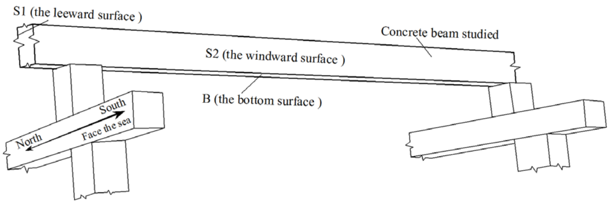

Fig. 2. Schematic diagram of beam.

The section of the concrete beam was 60 mm in width and 190 mm in depth, as shown in Fig. 3. After removing the beam from the structure, the compressive strength of the beam was tested as 22.6 MPa. The leeward surface and is labelled as S1, and the windward surface is labelled as S2. Part of the beam is cut and polished as shown in Fig. 3.

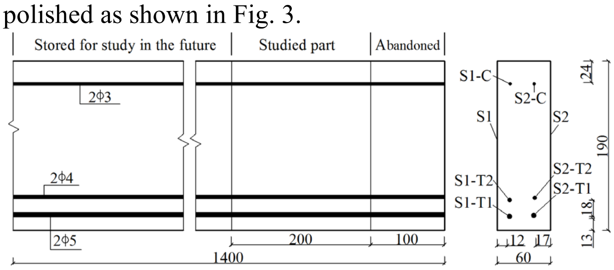

Fig. 3. Schematic diagram of the beam.

2.2 Sample Preparation

The part considered in this study was about 200 mm in the right part of the 1400mm beam shown in Fig. 3. It was cast into a low-viscosity epoxy resin to minimize artificial damage during cutting. After the hardening of the epoxy resin, a concrete cutting machine was applied to cut the part from the beam. The part was then immersion into low-viscosity epoxy resin and cut into six blocks. Both the width and depth of each block was about 25 mm. A steel bar was in the center of each block, as shown in Fig. 4. Then, an abrasive cutter (SYJ-200) was used to cut the six blocks into slices. The thickness of each slice was about 12-mm. The blocks were sliced with a speed of 0.05 mm/s during flushing with water. Subsequently, a polishing machine (UNIPOL-1502) was used to make the steel bar smooth. Then the slices were cleaned by an ultrasonic cleaner. To keep dry and isolate from air, each slice was placed in an vacuum-sealed bag.

After remove the damaged slices, about 8 slices were obtained for each block finally. These slices were labelled as Steel bar label－Number of the slice. Take the second slice of the steel bar C-T2 as the example, it was labelled as C-T2-2. More information about the beam and the sample preparation can be found in reference [11].

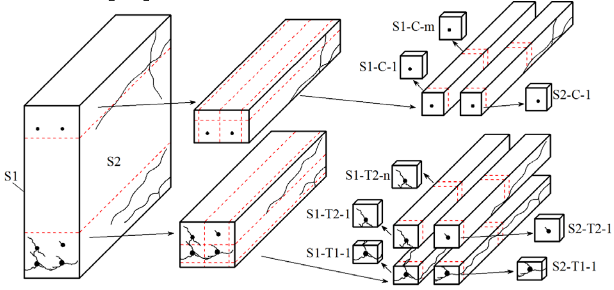

Fig. 4. Schematic diagram of the sample preparation.

2.3 Measurement on CP and CL

Two scanning electron microscope (SEM), QUANTA FEG650 and Hitachi S-3400, were applied to observe the samples. Five regions can be seen in the steel/concrete interface, which are steel, corrosion layer (CL), millscale (MS), corrosion-product-filled paste (CP), and concrete as shown in Fig. 5. The CL and CP were observed and pictured. The T_{CL} and T_{CP} was measured by a graphics processing software, Image-Pro Plus 6.0.

About 30 points were measured for each slice around the steel bar, evenly. For each sample, the average T_{CP} and the average T_{CL} of all the 30 measurement points were averaged separately. The results are shown and analyzed in Section 3.

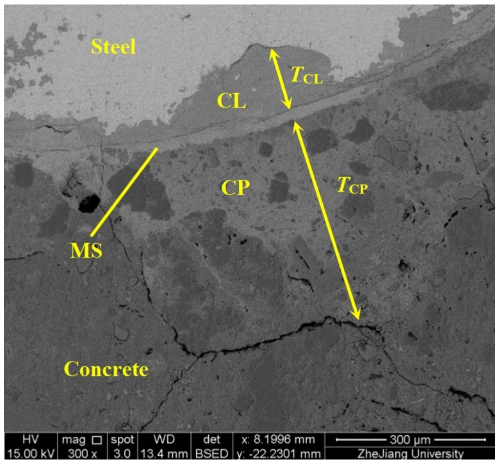

Fig.5. Distributions of corrosion product at steel－concrete interface.

https://doi.org/10.1051/e3sconf/202668602003

3 Experimental Results

3.1 The T_{CP} - T_{CL} model

The T_{CP} and T_{CL} at all measuring points were scattered. In order to determine the intrinsic relationship between T_{CP} and T_{CL}, the scattered data were graded at each 100 µm, base on the experience in reference [5]. The results are shown in Fig. 6.

The previous T_{CP}–T_{CL} model shows that the T_{CP} increases with T_{CL} at the beginning, and then T_{CP} no longer increase as the increase of T_{CL}, as illustrated in Fig. 1[5]. Obviously, the results shown in Fig. 6 are consistent with the T_{CP}–T_{CL} model, except for S1-C (Fig. 6(C)). This may be due to the corrosion of S1-C being too slight; therefore, T_{CP} would still increase with the T_{CL}. In fact, few cracks were found near the S1C surface. The maximum of T_{CL} is 237µm as shown in Fig. 6(c), which is smaller than the T_{CL}^{cr} of other steel bars. Thus, all points were linearly fitted in order to obtain k_T, and T_{CP}^{max} was not determined for S1-C.

It needs to be noted that the T_{CL} for the S2-T1 and S1-T2 were removed, because it is much larger than that of the other data. This may be due to the transverse cracks in the beam near these slices [11]. The cracks make the ingress of aggressive agents easier and accelerate the steel corrosion. Therefore, a sudden increase was found in the slices. With regard to S2-C, there were not enough points to be graded into groups when T_{CL} was larger than 500 µm; therefore, all points with T_{CL} larger than 500 µm were taken as a group to calculate the average value of T_{CP} and T_{CL}.

With regard to the other steel bars, the average T_{CP} value no longer exhibited significant growth, after the average T_{CL} became larger than 300 µm, as shown in Fig. 6. Thus, the points where T_{CL} was smaller than 300 µm were linearly fitted and k_T was obtained, and the points where T_{CL} was larger than 300 µm were given the average T_{CP} value in order to obtain T_{CP}^{max}. The corresponding T_{CL} at the intersection of the two fitted lines is T_{CL}^{cr}. The fitted lines and values of k_T, T_{CP}^{max}, and T_{CL}^{cr} are shown in Fig. 6. The k_T of S1-T1, S2-T1, S1-T2, S2-T2, S1-C and S2-C are 1.403, 2.301, 2.529, 2.680, 1.865 and 3.778, respectively. The T_{CP}^{max} of S1-T1, S2-T1, S1-T2, S2-T2 and S2-C are 367.4 µm, 736.6 µm, 521.1 µm, 711.9 µm and 1199 µm, respectively. The T_{CL}^{cr} of S1-T1, S2-T1, S1-T2, S2-T2 and S2-C are 261.9 µm, 320.2 µm, 206.0 µm, 265.6 µm and 317.4 µm, respectively.

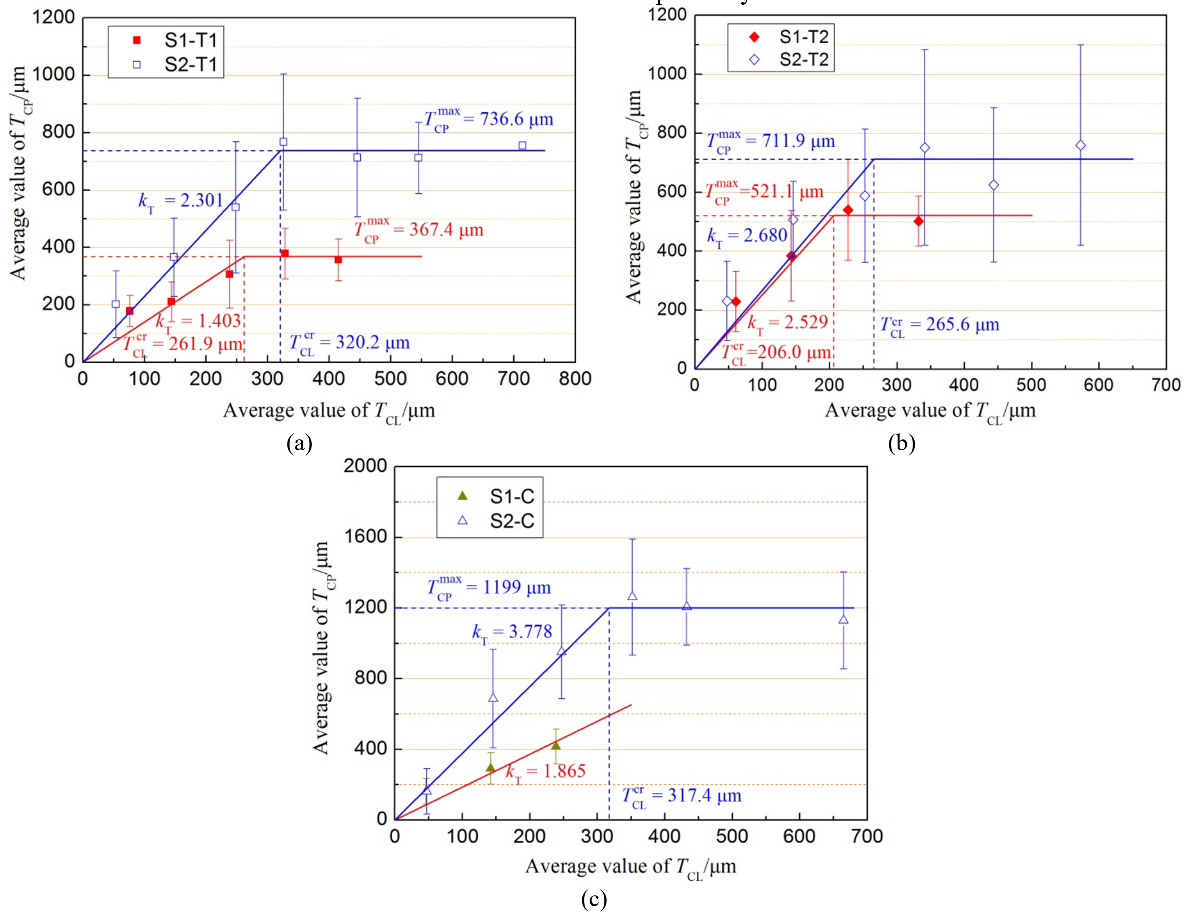

Fig. 6. Relationship between T_{CP} and T_{CL} of different series; (a) T1, (b) T2, and (c) C.

3.2 Parameters in the model

According to the Fig. 6(a), it can be observed that the k_T, T_{CP}^{max}, and T_{CL}^{cr}, of Series S2 (the windward surface), are larger than those of Series S1 (the leeward surface). The same conclusion can be drawn in Fig. 6 (b) and (c). The larger k_T means the faster propagation of CL at a certain value of T_{CP}. The larger T_{CP}^{max} means the further propagation of CP. S2 suffered more ingression of chloride and water due to the sea wind; therefore, the concrete in S2 had more chloride ions and larger humidity than S1, which made the penetration of Fe ions easier than in the case of S1. Thus, the penetration of Fe ions from the steel bar to the surrounding concrete is easier. Therefore, k_T and T_{CP}^{max} of Series S2, were larger than those of Series S1.

Comparison the results of Fig 6(a) and Fig. 6(b), it can be seen that the k_T, T_{CP}^{max}, and T_{CL}^{cr}, of Series T1 (outside steel bar), were larger than those of Series T2 (the inner steel bar), as for the steel bars from the same surface. This is consistent with the results of previous study [11], where the CL and CP grow faster in the tension region than in the compressive region of the beam. This was because both chloride ions and water ingress into the concrete of Series T1 from both the side and bottom of the beam. This made the penetration of Fe ions easier than in the case of T2. Moreover, the larger tensile stress in the concrete may induce micro-cracks in the concrete cover and have also accelerated the migration of Fe ions. Therefore, the values of k_T and T_{CP}^{max} of Series T1 (the outside steel bars), are larger than those of T2 (the inner steel bars).

4 Conclusions

This study investigated a beam which have serviced at coastal environment from 1970s to 2015. The beam was cut into several blocks with a steel bar in each block. The concrete/steel interface was observed by SEM to study the distribution of corrosion-filled-paste and corrosion layer. The following conclusions can be drawn from the study:

(1) A T_{CP}–T_{CL} model in marine atmosphere is proposed, which provides a mechanistic basis for predicting corrosion evolution and guiding maintenance strategies for aging marine concrete structures.

(2) The steel corrosion and values of k_T and T_{CP}^{max}, in the T_{CP}–T_{CL} model of the steel bars, near the windward surface, are larger than those near the leeward surface.

(3) The steel corrosion and values of k_T and T_{CP}^{max}, in the T_{CP}–T_{CL} model of the outside steel bars, are larger than those of the inner steel bars.

Reference

1. Yu S , Liu Q , Hong F ,et al.Crystal structure-dependent evaluation of chloride ions resistance of iron passivation film in reinforced concrete at the nanoscale[J].Journal of Building Engineering, 2024, 95(000).
2. T.D. Marcotte, C.M. Hansson, Corrosion products that form on steel within cement paste, Mater. Struct. 40 (2007) 325-340.
3. Xu L , Wu P , Zhu X ,et al.Structural characteristics and chloride intrusion mechanism of passive film[J]. Corrosion Science, 2022, 207.
4. Dang L M , Wang H , Li Y ,et al.Deep learning-based masonry crack segmentation and real-life crack length measurement[J].Construction and Building Materials, 2022.
5. Y. Zhao, H. Ding, W. Jin. Development of the corrosion-filled paste and corrosion layer at the steel/concrete interface, Corros. Sci., 87 (2014) 199-210.
6. Wang P , Qiao H , Zhang Y ,et al.Three-dimensional characteristics of steel corrosion and corrosion-induced cracks in magnesium oxychloride cement concrete monitored by X-ray computed tomography[J].Construction and Building Materials, 2020, 246:118504.
7. Robuschi S , Tengattini A , Dijkstra J ,et al.A closer look at corrosion of steel reinforcement bars in concrete using 3D neutron and X-ray computed tomography[J].Cement and Concrete Research, 2021, 144:106439.
8. Tian Y, Jiang H, Fan X, et al. Corrosion damages of reinforced concrete characterized by X-ray CT and DVC techniques,Construction and Building Materials,2023,409.
9. Wang Y , Miao X , Zhao Y ,et al.Quantitative image analysis on the filling proportion of corrosion products in reinforced concrete using X-ray computed tomography[J].Cement and Concrete Composites, 2024, 150(000):18.
10. Zhang X , Jin H , Yu S ,et al.Analysis of bending deflection of tunnel segment under load- and corrosion-induced cracks by improved XFEM[J]. Engineering Failure Analysis, 2022.
11. Dong J , Lin X , Liu X ,et al.Distribution of Steel Corrosion Products in a Cracked Concrete Beam Exposed to Coastal Atmosphere[J]. Springer, Singapore, 2025.